
Article:
Paspatis, A.G. orcid.org/0000-0002-3479-019X, Konstantopoulos, G.C. orcid.org/0000-0003-3339-6921 and Guerrero, J.M. (2021) Enhanced current-limiting droop controller for grid-connected inverters to guarantee stability and maximize power injection under grid faults. IEEE Transactions on Control Systems Technology, 29 (2). pp. 841-849. ISSN 1063-6536

https://doi.org/10.1109/TCST.2019.2955920

Enhanced Current-Limiting Droop Controller for Grid-Connected Inverters to Guarantee Stability and Maximize Power Injection under Grid Faults

Alexandros G. Paspatis, *Student Member, IEEE,* George C. Konstantopoulos, *Member, IEEE,* and Josep M. Guerrero, *Fellow, IEEE*

***Abstract*—Droop controlled inverters are widely used to integrate distributed energy resources (DERs) to the smart grid and provide ancillary services (frequency and voltage support). However, during grid variations or faults, the droop control scheme should inherit a current-limiting property to protect both the inverter and the DER unit. In this brief, a novel structure of the recently developed current-limiting droop (CLD) controller is proposed to accomplish two main tasks: i) guarantee current limitation with maximum power injection during grid faults and ii) rigorously guarantee asymptotic stability of any equilibrium point in a given bounded operating range of the closed-loop system for a grid-connected inverter. Since the maximum power of the DER unit can be utilized under grid faults with the proposed enhanced CLD, then inspired by the latest fault-ride-through requirements, it is further extended to provide voltage support to a faulty grid via the maximum injection of reactive power. This is achieved by simply adjusting the reactive power reference opposed to existing control schemes which require adjustment of both the real and the reactive power. Hence, a unified current-limiting control scheme for grid-connected inverters under both normal and faulty grids with a simplified voltage support mechanism is developed and experimentally verified in this brief.**

***Index Terms*—Nonlinear control, inverter, droop control, current-limiting property, stability analysis, voltage support, voltage sags.**

I. Introduction

DROOP controlled inverters play a key role in modern smart grids, where adaptability and autonomy represent essential properties for every inverter that interfaces a distributed energy resource (DER) to the grid [1]. Inspired by the response of conventional synchronous generators to grid voltage and frequency variations, droop control has been adopted by inverters to provide voltage and frequency support, via adjusting the injected real and reactive power [2]. The droop control methodology has dominated the control system of inverters and still represents an active area of research in terms of improving its dynamic performance using a virtual impedance [3] or by adjusting the droop parameters [4]. In the same framework, a universal droop controller has been proposed in [5] that regulates the voltage and frequency of the grid independently of the output impedance of the inverter; thus significantly enhancing system robustness.

However, in addition to the desired droop control operation, the stability of droop controlled inverters must be guaranteed at all times [6], [7]. Since the power measurements that are required for the droop control operation introduce nonlinear dynamics into the control system, the linearization method (small-signal model) is often employed in order to investigate the stability of a droop controlled inverter [8]. In the vast majority of these cases, the stability analysis is based on a root locus approach for the controller parameters, where the accurate values of the inverter and grid/load parameters are assumed to be known [5]. Even when the parameters of the system are accurately known, which is not always true in practice, the stability proof is conducted only for a given inverter application. Hence, there is a need for designing droop controllers for inverter-interfaced units that ensure the stability of any equilibrium point within a given operating range independently from the system parameters. For inverter-based microgrids, conditions for stability have been presented in [9] without requiring knowledge of the system parameters while in [10], voltage stability is guaranteed using a nonlinear quadratic droop control. Nevertheless, several assumptions on the system characteristics are often taken into account to ensure stability, such as a lossless network structure and small or bounded power angles [9], [11], [12].

Although stability is an essential property of droop controlled inverters, the protection of the inverter device is also of great importance especially under faulty conditions. Maintaining the inverter current below its predefined maximum value is an essential requirement in order to avoid damages in the power components. To this end, current-limiting techniques have been proposed for grid-connected inverters in [13], [14] or for inverter-interfaced microgrids in [15], [16] and ensure a current limitation either through current control or by introducing a virtual resistance. However, these techniques either assume fast regulation or require saturation units, external limiters or a switching action between different dynamic control schemes under normal and faulty grid conditions, which may lead to instability, as discussed in [17], [18], [19]. In [20], it is shown that when switching between the original and the current-limiting controller occurs, two undesirable phenomena may arise, i.e. integrator wind-up and latch-up. In order to overcome these issues, it is important to obtain a unified control scheme that incorporates a current-limiting property within the droop control and thus, avoid switching between different dynamic controllers. Recently, a droop controller that can ensure a current limitation under a maximum value at all times, without any switching operation, was proposed for grid-tied inverters [21]. However, the controller proposed in

This work was supported by the EPSRC under Grants No. EP/S001107/1 and EP/S031863/1.

A.G. Paspatis and G.C. Konstantopoulos are with the Department of Automatic Control and Systems Engineering, The University of Sheffield, Sheffield, S1 3JD, UK. E-mails: {apaspatis1,g.konstantopoulos}@sheffield.ac.uk.

J.M. Guerrero is with with the Department of Energy Technology, AAU, 9220 Aalborg East, Denmark. E-mail: joz@et.aau.dk.

[21] cannot utilize the full capacity of the inverter under faults and hence, the current is limited to a value lower than the maximum when a fault occurs depending on the grid voltage sag. According to the current grid codes, the capacity of the DERs connected to the grid should be utilized under faults in order to support the grid voltage and avoid the instant tripping of DERs [22], [23], [24], [25]. In this context, Fault-Ride-Through (FRT) requirements have been recently introduced to standardize the way DERs support the voltage at their connection point, by injecting reactive power depending to the voltage drop percentage [26].

In this brief, the droop control design for grid-connected inverters with current-limiting characteristics is revisited and an enhanced version of the current-limiting droop controller is proposed. Using ultimate boundedness analysis, it is analytically proven that the proposed controller can guarantee the desired current-limiting property at all times, even under transient phenomena, without using any saturation units or depending on the system parameters. This current limitation is proven independently from the grid voltage variations; thus enabling maximum power utilization under grid faults. In addition, the asymptotic stability of any equilibrium point of the closed-loop system within a given operating range is proven for the first time with the proposed controller. Hence, compared to the original CLD controller presented in [21], the novel contributions of the proposed enhanced CLD controller include: i) new controller structure and dynamics that guarantee the desired limitation and can utilize the maximum power capacity of the inverter under grid faults, i.e. the inverter current reaches the maximum allowed value during faults, ii) the asymptotic stability of the closed-loop system, is proven for first time in this brief using a current-limiting droop controller independently of the system parameters. It is worth mentioning that opposed to existing stability proofs that assume a small (or bounded) power angle [11], [12], according to the authors knowledge, this is the first time that the boundedness of the power angle is guaranteed by the control design and does not represent an assumption. Finally, since the maximum power capacity of the inverter (or equivalently the DER unit) can be utilized under faults, the final contribution of this brief includes an extension of the proposed enhanced CLD to provide voltage support under faults by injecting maximum reactive power (inspired by FRT requirements). In contrast to existing voltage support methods that adjust both the real and the reactive power reference [27], [28], the proposed control scheme introduces only a change of the reactive power reference to accomplish the same tasks. The efficacy of the proposed control approach is validated with extended experimental results for a grid-connected inverter under both normal and faulty grid conditions.

II. System modeling and problem description

The power system under consideration is a single-phase inverter connected to the grid through an LCL filter, as depicted in Fig. 1. The capacitor of the filter is denoted as C while the inductances are denoted as L and L_g with parasitic resistances r and r_g, respectively. The output voltage and current of the inverter are v and i, while the capacitor voltage

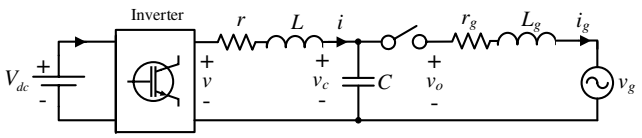

Figure 1. The inverter connected to the grid via an LCL filter

is denoted as v_c. The voltage and current of the grid are v_g and i_g with $v_g = \sqrt{2}V_g \sin\omega_g t$, where V_g is the RMS grid voltage and ω_g is the angular grid frequency.

The dynamic equations of the system can be obtained as

$$\begin{aligned} L\frac{di}{dt} &= v - v_c - ri \\ C\frac{dv_c}{dt} &= i - i_g \\ L_g\frac{di_g}{dt} &= v_c - v_g - r_g i_g \end{aligned} \tag{1}$$

where v represents the control input and corresponds to the voltage at the output of the inverter.

Although the plant (1) is linear, the complexity of analyzing a grid-connected inverter increases due to the nonlinearities of the control dynamics, which arise from the calculation of the real power P and reactive power Q, such as in the case of the droop control. Different droop control schemes have been proposed in the literature; however, the current-limiting droop control proposed in [21] adopts the $P \sim V$ and $Q \sim -\omega$ droop expressions of the universal robust droop controller [5], which have been shown to hold independently of the output impedance. Hence, a desired current limitation under a maximum value is achieved without using saturated integrators that can lead to instability by incorporating the bounded integral control (BIC) structure, developed in [29], which mimics the response of a saturated integral controller but does not suffer from integrator wind-up.

The significant drawback of the original CLD controller [21] is that the maximum capacity of the inverter is not utilized under voltage sags. In fact, only a limited amount of power can be injected to the grid during faults which corresponds to the percentage of the voltage drop. For example, in a short circuit scenario, the injected current will be zero, which is similar to disconnecting the inverter. Thus the inverter cannot support the grid voltage under faults. In addition, the asymptotic stability of the closed-loop system has not been proven yet and therefore the stable operation of the grid-connected inverter cannot be guaranteed. To this end, a novel enhanced current-limiting droop controller that overcomes all the above limitations is presented in the sequel.

III. The Proposed Controller

The main goal in this paper is to propose a droop controller that inherently limits the inverter current to protect the device under unrealistic power demands or under grid faults, while supporting the grid voltage at all times. Hence, inspired by the structure of the original CLD in [21], a dynamic virtual resistance is introduced in series with the filter inductor through the control input v, which should remain positive and bounded. Although this bounded dynamic virtual resistance

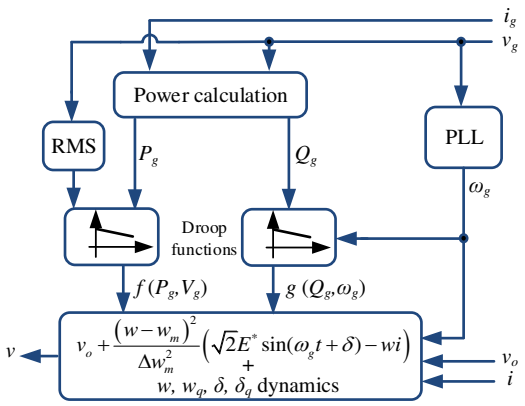

Figure 2. Proposed controller implementation

can be implemented using traditional integral control with saturation, such an approach can lead to integrator wind-up and instability [17]. Therefore, the bounded integral control (BIC) concept proposed in [29] is utilized here to overcome this limitation. Finally, due to the virtual resistance introduced from the control design, the $P \sim V$ and $Q \sim -\omega$ droop expressions of the universal droop controller are employed [5], [30]. Keeping in mind these facts, in order to overcome the limitations of the original CLD mentioned in the previous section, the novel control structure of the current-limiting droop controller proposed in this work takes the form:

$$v = v_o + \frac{(w-w_m)^2}{\Delta w_m^2}\left(\sqrt{2}E^*\sin(\omega_g t+\delta) - wi\right), \quad (2)$$

with control dynamics

$$\begin{bmatrix} \dot{w} \\ \dot{w}_q \end{bmatrix} = \begin{bmatrix} 0 & -c_w f(P_g,V_g) w_q^{2l-1} \\ \frac{c_w w_q}{l\Delta w_m^2} f(P_g,V_g) & -\frac{k_w}{l}\left(\frac{(w-w_m)^2}{\Delta w_m^2}+w_q^{2l}-1\right) \end{bmatrix} \begin{bmatrix} w-w_m \\ w_q \end{bmatrix} \quad (3)$$

$$\begin{bmatrix} \dot{\delta} \\ \dot{\delta}_q \end{bmatrix} = \begin{bmatrix} 0 & c_\delta g(Q_g,\omega_g)\delta_q^{2l-1} \\ -\frac{c_\delta \delta_q}{l\Delta\delta_m^2} g(Q_g,\omega_g) & -\frac{k_\delta}{l}\left(\frac{\delta^2}{\Delta\delta_m^2}+\delta_q^{2l}-1\right) \end{bmatrix} \begin{bmatrix} \delta \\ \delta_q \end{bmatrix} \quad (4)$$

where $l \geq 1 \in \mathcal{N}$ and $f(P_g,V_g)$ and $g(Q_g,\omega_g)$ are given by

$$f(P_g,V_g) = n(P_{set}-P_g)+K_e(E^*-V_g) \quad (5)$$

$$g(Q_g,\omega_g) = m(Q_g-Q_{set})+\omega^*-\omega_g \quad (6)$$

and represent the droop control expressions, with c_w, c_δ, k_w, k_δ, w_m, Δw_m and $\Delta\delta_m$ being positive constant parameters of the controller, E^* and ω^* being the rated grid voltage and frequency and n, m representing the droop coefficients. The initial conditions are defined as $w_0 = w_m, w_{q0} = 1$ and $\delta_0 = 0, \delta_{q0} = 1$.

As it is obvious from Fig. 1, when the inverter is not connected to the grid, then $v_o = v_g$ and when the relay closes, $v_o = v_c$. Parameters w and δ represent a virtual resistance and phase shift, respectively, which vary according to the nonlinear dynamic expressions (3)-(4). In order to guarantee boundedness of the controller states w, w_q, δ and δ_q without using saturation units, a generalized version of the BIC [29], is proposed in this brief depending on the value of $l \geq 1 \in \mathcal{N}$. To further explain this, one can consider the functions $W_w = \frac{(w-w_m)^2}{\Delta w_m^2}+w_q^{2l}$ and $W_\delta = \frac{\delta^2}{\Delta\delta_m^2}+\delta_q^{2l}$ for systems (3) and (4), respectively, and following similar analysis with [19], [21], [29], [31], it can be easily proven that the controller states w, w_q and δ, δ_q will start and remain on the sets $E_w = \left\{w, w_q \in R : \frac{(w-w_m)^2}{\Delta w_m^2}+w_q^{2l}=1\right\}$ and $E_\delta = \left\{\delta, \delta_q \in R : \frac{\delta^2}{\Delta\delta_m^2}+\delta_q^{2l}=1\right\}$, based on the given initial conditions. Thus, it holds that $w \in [w_{min}, w_{max}] > 0$ and $\delta \in [-\Delta\delta_m, \Delta\delta_m]$ for all $t \geq 0$. Note that for $l = 1$, the dynamics (3)-(4) take the form of the original BIC [29], while $w_{min} = w_m - \Delta w_m$, $w_{max} = w_m + \Delta w_m$, $\Delta\delta_m$ can be set by the control operator and represent the minimum and maximum values of the virtual resistance and the maximum absolute value of the phase shift, respectively.

Regarding the selection of the rest of the controller parameters, the variables c_w and c_δ represent the controller integral gains and the variables k_w and k_δ are used to increase the robustness of the control states w_q and δ_q. These parameters can be selected according to the analysis in [21]. Furthermore, note that $w_0 = w_m$ corresponds to the initial current I_m that flows through the LC filter when the switch in Fig. 1 is open (before grid connection) and thus, it can be selected as $w_m = \frac{E^*}{I_m} = \frac{E^*}{\omega_g C V_g}\sqrt{(1-\omega_g^2 LC)^2+(r\omega_g C)^2}$.

By removing the terms $K_e(E^*-V_g)$ and $\omega^*-\omega_g$ from equations (5) and (6), the proposed controller can easily change its operation from the PQ-droop mode to the PQ-set mode in order to regulate the real and reactive power at their reference values. It is underlined that, compared to the original CLD in [21], here the proposed enhanced controller introduces the generalized nonlinear dynamics (3)-(4) and a different expression for the control input v given in (2). In particular, the proposed inverter voltage v depends only on the virtual resistance w and the phase shift δ (controller states) and makes use of the rated value E^* of the voltage. The new structure of the controller ensures that the maximum power capacity of the inverter is utilized under faults and facilitates a rigorous stability analysis, as shown in the section that follows, which represent two of the key contributions of this brief.

IV. Stability Analysis

A. Current-limiting property

By applying the proposed controller (2) into the original system dynamics (1) and assuming grid-connected operation where $v_o = v_c$, the closed-loop dynamics of the inverter current become

$$L\frac{di}{dt} = -ri - \frac{(w-w_m)^2}{\Delta w_m^2}wi + \frac{(w-w_m)^2}{\Delta w_m^2}\sqrt{2}E^*\sin(\omega_g t+\delta). \quad (7)$$

For system (7), consider the continuous differentiable function V representing the energy stored in the inductor L, i.e.

$$V = \frac{1}{2}Li^2. \quad (8)$$

Since $w \in [w_{min}, w_{max}] > 0$ for all $t \geq 0$ according to the boundedness property of the generalized BIC explained above, the time derivative of V is calculated as

$$\begin{aligned} \dot{V} &= -ri^2 - \frac{(w-w_m)^2}{\Delta w_m^2}wi^2 + \frac{(w-w_m)^2}{\Delta w_m^2}\sqrt{2}E^* i\sin(\omega_g t+\delta) \\ &\leq -ri^2 - \frac{(w-w_m)^2}{\Delta w_m^2}w_{min}i^2 + \frac{(w-w_m)^2}{\Delta w_m^2}\sqrt{2}E^*|i||\sin(\omega_g t+\delta)| \\ &\leq -ri^2, \forall\, |i| \geq \frac{\sqrt{2}E^*}{w_{min}}. \end{aligned}$$

Thus, according to the Theorem 4.18 in [32], there exists a $\mathcal{KL}$ function β so that for any initial condition $i(0)$, there is a $T \geq 0$ such that

$$|i(t)| \leq \beta(|i(0)|, t) \quad \forall 0 \leq t \leq T$$
$$|i(t)| \leq \frac{\sqrt{2}E^*}{w_{min}} \qquad \forall t \geq T,$$

proving that the solution of the inverter current is uniformly ultimately bounded. Note that if initially $|i(0)| \leq \frac{\sqrt{2}E^*}{w_{min}}$, then $T = 0$, i.e. it holds true that

$$|i(t)| \leq \frac{\sqrt{2}E^*}{w_{min}}, \forall t \geq 0. \tag{9}$$

Since w_{min} is linked to the controller parameters ($w_{min} = w_m - \Delta w_m$), which are designed by the user, then by selecting

$$w_{min} = \frac{E^*}{I_{max}} \tag{10}$$

it yields

$$|i(t)| \leq \sqrt{2}I_{max}, \forall t \geq 0. \tag{11}$$

The previous inequality holds for any $t \geq 0$ and for any constant positive I_{max}. As a result

$$I \leq I_{max}, \forall t \geq 0, \tag{12}$$

where I is the RMS value of the inverter current, showing that the proposed controller introduces a current-limiting property below a given value I_{max}, that can be selected by the control operator. Since inequalities (9) and (12) do not depend on the grid voltage or frequency, i.e. V_g or ω_g, it is clear that the proposed controller can limit the RMS value of the current under I_{max} irrespectively of grid variations or faults, utilizing the maximum power capacity of the inverter at all times. This is a significant advantage compared to the original CLD.

B. Asymptotic stability

In the previous subsection, the dynamic model (1) was used to prove the desired current limitation for the instantaneous value of the current, irrespective of the functions $f(P_g, V_g)$ and $g(Q_g,\omega_g)$; hence, the current-limiting property holds at all times, even during transients. However, to investigate whether the closed-loop system can regulate the real and reactive power or operate under the droop control mode, the functions $f(P_g, V_g)$ and $g(Q_g,\omega_g)$ should be considered in the analysis.

Note that for a single-phase inverter, the P_g and Q_g expressions represent the average real and reactive power of the inverter. Hence, as it is shown in [9], [11], [33], in order to analyze the stability of a droop-controlled single-phase inverter, the expressions of P_g and Q_g that use the RMS voltages and the power angles, i.e. the phasor voltages, should be utilized. This approach can be used in this work since the inverter frequency does not introduce additional dynamics due to the utilization of the PLL to obtain ω_g (PLL response is much faster than the inverter and droop control dynamics [34] and hence the phasor analysis makes sense).

As it can be seen from (7), the dynamics of the inverter current, when grid-connection has been achieved, are partially decoupled from the capacitor voltage and grid current dynamics due to the feed-forward term v_c used in (2). Thus, the equivalent circuit of the grid-connected inverter takes the form shown in Fig. 3. Here,

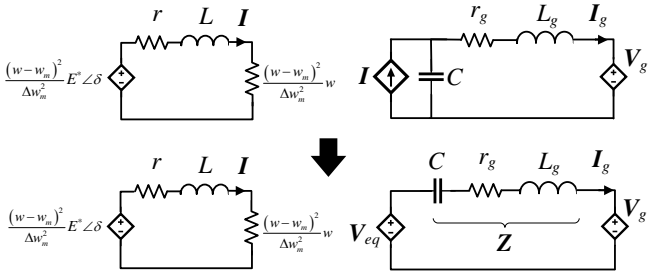

Figure 3. Equivalent circuit of the closed-loop system.

$$\boldsymbol{V}_{eq} = -jX_C\boldsymbol{I}$$

where $X_c = \frac{1}{\omega_g C}$ and

$$\boldsymbol{I} = \frac{E^* \frac{(w-w_m)^2}{\Delta w_m^2}\angle\delta}{\frac{(w-w_m)^2}{\Delta w_m^2}w + r + j\omega_g L}.$$

Considering that $\boldsymbol{V}_g = V_g\angle 0^o$, then the real and reactive power delivered at the grid are given from the following expressions explained in [33] and [35]:

$$P_g = -\frac{V_g^2}{Z}cos(\theta_Z) + \frac{V_g E^* (w-w_m)^2 X_c}{\Delta w_m^2 \sqrt{\left(\frac{(w-w_m)^2}{\Delta w_m^2}w + r\right)^2 + (\omega_g L)^2 Z}}cos(\varphi) \tag{13}$$

$$Q_g = -\frac{V_g^2}{Z}sin(\theta_Z) - \frac{V_g E^* (w-w_m)^2 X_c}{\Delta w_m^2 \sqrt{\left(\frac{(w-w_m)^2}{\Delta w_m^2}w + r\right)^2 + (\omega_g L)^2 Z}}sin(\varphi), \tag{14}$$

with $\mathbf{Z} = Z\angle\theta_Z = \sqrt{r_g^2 + \left(\omega_g L_g - \frac{1}{\omega_g C}\right)^2}\angle tan^{-1}\left(\frac{\omega_g L_g - \frac{1}{\omega_g C}}{r_g}\right)$ and $\varphi = \delta - tan^{-1}\left(\frac{\omega_g L}{\frac{(w-w_m)^2}{\Delta w_m^2}w + r}\right) - \theta_Z - \frac{\pi}{2}$. Since δ is bounded, i.e. $\delta \in [-\Delta\delta_m, \Delta\delta_m]$, then φ is also bounded and can take positive or negative values to allow the inverter to inject or receive reactive power from the grid. Thus, without loss of generality, we can assume that $\varphi \in \left(-\frac{\pi}{2}, \frac{\pi}{2}\right)$ and $\omega_g^2 L_g C < 1$.

The closed-loop dynamics for the stability analysis can be obtained by combining (3)-(6) with (13)-(14) and the state vector is given as $x = [w\, w_q\, \delta\, \delta_q]^T$. Note that by considering constant V_g and ω_g (not necessarily equal to their rated values), an equilibrium point $x_e = [w_e\, w_{qe}\, \delta_e\, \delta_{qe}]^T$ of the closed-loop system can be obtained. Hence, the stability properties of the grid-connected inverter under the proposed enhanced CLD are summarized in the following proposition.

Proposition 1. *Every equilibrium point $x_e = [w_e\, w_{qe}\, \delta_e\, \delta_{qe}]^T$ of the closed-loop system obtained by* (3)-(6) *and* (13)-(14)*, with $w_e \in \left(w_{min}, \frac{w_m}{3}\right)$ and $\delta_e \in (-\Delta\delta_m, \Delta\delta_m)$ is asymptotically stable when $\Delta\delta_m$ is selected as*

$$\Delta\delta_m = \min\left\{\left|\max\left\{0, \frac{\pi}{2} + \tan^{-1}\left(\frac{2\left((w_{min}+r)^2 + (\omega_g L)^2\right)}{\omega_g L(3w_{min} - w_m)} - \frac{w_{min}+r}{\omega_g L}\right)\right\} + \right.$$
$$\left. + \tan^{-1}\left(\frac{\omega_g L}{w_{min}+r}\right) + \theta_Z\right|, \pi + \tan^{-1}\left(\frac{27\omega_g L \Delta w_m^2}{4w_m^3 + 27\Delta w_m^2 r}\right) + \theta_Z\right\}. \tag{15}$$

Proof: Considering any equilibrium point $x_e = [w_e\, w_{qe}\, \delta_e\, \delta_{qe}]^T$ with $w_e \in \left(w_{min}, \frac{w_m}{3}\right)$ and $\delta_e \in$

$(-\Delta\delta_m, \Delta\delta_m)$, the Jacobian matrix of the system takes the form

$$A = \begin{bmatrix} A_T & 0_{2x1} & 0_{2x1} \\ A_1 & -2k_w w_{qe}^{2l} & 0 \\ A_2 & 0 & -2k_\delta \delta_{qe}^{2l} \end{bmatrix},$$

where

$$A_T = \begin{bmatrix} -a\zeta\cos(\varphi_e) - \frac{a\omega_g L\psi\Delta w_m^2}{\varepsilon}\sin(\varphi_e) & -a\,(w_e - w_m)^2\sin(\varphi_e) \\ b\zeta\sin(\varphi_e) - \frac{b\omega_g L\psi\Delta w_m^2}{\varepsilon}\cos(\varphi_e) & -b\,(w_e - w_m)^2\cos(\varphi_e) \end{bmatrix}$$

with $\varepsilon = \left(\left(\frac{(w_e - w_m)^2}{\Delta w_m^2} w_e + r\right)^2 + (\omega_g L)^2\right)\Delta w_m^4$, $a = \frac{c_w n V_g E^* w_{qe}^{2l}}{\omega_g C\sqrt{\varepsilon} Z}$, $b = \frac{c_\delta m V_g E^* \delta_{qe}^{2l}}{\omega_g C\sqrt{\varepsilon} Z}$, $\psi = (w_e - w_m)^3\,(3w_e - w_m)$, $\gamma = \left(\frac{(w_e - w_m)^2}{\Delta w_m^2} w_e + r\right)\Delta w_m^2\psi$ and $\zeta = \frac{\gamma}{\varepsilon} - 2\,(w_e - w_m)$. Since $w_e \in \left(w_{min}, \frac{w_m}{3}\right)$ and $\delta_e \in (-\Delta\delta_m, \Delta\delta_m)$, then $w_{qe}, \delta_{qe} \in (0, 1]$ and therefore $-2k_w w_{qe}^{2l} < 0$ and $-2k_\delta \delta_{qe}^{2l} < 0$ (for details see [21]). Hence, the eigenvalues of A will have negative real parts if the eigenvalues of A_T have negative real parts. The characteristic polynomial that is derived from the characteristic equation $\det[\lambda I - A_T] = 0$ takes the form

$$\lambda^2 + \lambda\Big(\Big(b(w_e - w_m)^2 + a\zeta\Big)\cos(\varphi_e) + \frac{a\omega_g L\psi\Delta w_m^2}{\varepsilon}\sin(\varphi_e)\Big) + ab\zeta\,(w_e - w_m)^2 = 0.$$

Since $ab\zeta\,(w_e - w_m)^2 > 0$, then x_e is asymptotically stable if

$$\Big(b(w_e - w_m)^2 + a\zeta\Big)\cos(\varphi_e) + \frac{a\omega_g L\psi\Delta w_m^2}{\varepsilon}\sin(\varphi_e) > 0 \tag{16}$$

is satisfied. Since $\varphi_e \in \left(-\frac{\pi}{2}, \frac{\pi}{2}\right)$, then

$$\tan^{-1}\left(\frac{\omega_g L}{\frac{(w_e - w_m)^2}{\Delta w_m^2} w_e + r}\right) + \theta_Z < \delta_e < \pi + \tan^{-1}\left(\frac{\omega_g L}{\frac{(w_e - w_m)^2}{\Delta w_m^2} w_e + r}\right) + \theta_Z. \tag{17}$$

The term $b\,(w_e - w_m)^2\cos(\varphi_e)$ is always positive and by substituting all the considered variables, (16) will hold true if

$$\tan(\varphi_e) > \frac{2\Delta w_m^2\left(\left(\frac{(w_e - w_m)^2}{\Delta w_m^2} w_e + r\right)^2 + (\omega_g L)^2\right)}{\omega_g L\,(w_e - w_m)^2\,(3w_e - w_m)} - \frac{\left(\frac{(w_e - w_m)^2}{\Delta w_m^2} w_e + r\right)}{\omega_g L} \tag{18}$$

yielding

$$\delta_e > \tan^{-1}\left(\frac{\omega_g L}{\frac{(w_e - w_m)^2}{\Delta w_m^2} w_e + r}\right) + \theta_Z + \frac{\pi}{2} + \tan^{-1}\left(\frac{2\Delta w_m^2\left(\left(\frac{(w_e - w_m)^2}{\Delta w_m^2} w_e + r\right)^2 + (\omega_g L)^2\right)}{\omega_g L\,(w_e - w_m)^2\,(3w_e - w_m)} - \frac{\left(\frac{(w_e - w_m)^2}{\Delta w_m^2} w_e + r\right)}{\omega_g L}\right). \tag{19}$$

By combining inequalities (17) and (19), the condition that δ_e needs to satisfy in order to guarantee asymptotic stability becomes

$$\max\left\{0, \frac{\pi}{2} + \tan^{-1}\left(\frac{2\Delta w_m^2\left(\left(\frac{(w_e - w_m)^2}{\Delta w_m^2} w_e + r\right)^2 + (\omega_g L)^2\right)}{\omega_g L\,(w_e - w_m)^2\,(3w_e - w_m)} - \frac{\left(\frac{(w_e - w_m)^2}{\Delta w_m^2} w_e + r\right)}{\omega_g L}\right)\right\} + \tan^{-1}\left(\frac{\omega_g L}{\frac{(w_e - w_m)^2}{\Delta w_m^2} w_e + r}\right) + \theta_Z < \delta_e < \pi + \tan^{-1}\left(\frac{\omega_g L}{\frac{(w_e - w_m)^2}{\Delta w_m^2} w_e + r}\right) + \theta_Z. \tag{20}$$

Since $w_e \in \left(w_{min}, \frac{w_m}{3}\right)$, then (20) will be always satisfied if the following condition holds:

$$\max\left\{0, \frac{\pi}{2} + \tan^{-1}\left(\frac{2\left((w_{min} + r)^2 + (\omega_g L)^2\right)}{\omega_g L(3w_{min} - w_m)} - \frac{w_{min} + r}{\omega_g L}\right)\right\} + \tan^{-1}\left(\frac{\omega_g L}{w_{min} + r}\right) + \theta_Z < \delta_e < \pi + \tan^{-1}\left(\frac{27\omega_g L\Delta w_m^2}{4w_m^3 + 27\Delta w_m^2 r}\right) + \theta_Z, \tag{21}$$

where $w_{min} = \frac{E^*}{I_{max}}$ according to (10) and $w_m = w_{min} + \Delta w_m$. Taking into account that $-\Delta\delta_m < \delta_e < \Delta\delta_m$ from the proposed controller dynamics and $w_e \in \left(w_{min}, \frac{w_m}{3}\right)$, then if $\Delta\delta_m$ is selected from (15), it is concluded that (21) is always satisfied guaranteeing asymptotic stability for the considered equilibrium point x_e. ■

Remark 2. Compared to the existing approaches that consider the assumption of small power angle to guarantee stability, here the bound for the phase shift δ is guaranteed via the control design and does not represent an assumption.

For typical values of L, E^* and I_{max} in low power-rating grid-connected inverter applications, where also small parasitic resistances r and r_g are considered, the term $\frac{2\left((w_{min} + r)^2 + (\omega_g L)^2\right)}{\omega_g L(3w_{min} - w_m)} - \frac{w_{min} + r}{\omega_g L}$ takes small values and $\theta_Z \approx -\frac{\pi}{2}$. Therefore, from (21), it is clear that $\Delta\delta_m$ can be simply selected as $\Delta\delta_m = \frac{\pi}{2}$. In practice, a slightly lower value than $\frac{\pi}{2}$ can be used to compensate the very small terms $\tan^{-1}\left(\frac{\omega_g L}{w_{min} + r}\right)$ and $\tan^{-1}\left(\frac{27\omega_g L\Delta w_m^2}{4w_m^3 + 27\Delta w_m^2 r}\right)$. However, for inverters with higher power ratings, the original expression (21) should be used to realize $\Delta\delta_m$.

Remark 3. Proposition 1 shows that asymptotic stability is guaranteed for any equilibrium point where $w_e \in \left(w_{min}, \frac{w_m}{3}\right)$. This corresponds to the range of the inverter RMS current $3I_m < I_e < I_{max}$, i.e. $\frac{3\omega_g C V_g}{\sqrt{\left(1 - \omega_g^2 LC\right)^2 + (r\omega_g C)^2}} < I_e < I_{max}$, which shows that the smaller the filter capacitor C the largest the operating range for the inverter current with guaranteed asymptotic stability.

V. Extending the Proposed Controller to Inherit Voltage Support Capability under Grid Faults

As proven in Section IV-A, the maximum power capability of the inverter can be now utilized with the proposed controller. Thus, inspired by the FRT requirements that have been proposed for DERs connected to the transmission and distribution networks, the proposed controller can be extended to provide support to the grid voltage under faults. As showcased in different FRT applications [26], voltage support is demanded when the voltage at the point of common coupling drops under 0.9 p.u. and it is practically accomplished through injection of reactive power. In order to introduce the voltage support mode (VSM) into the control design, expression (6) is proposed to take the form:

$$g(Q_g, a_f, \omega_g) = m(Q_g - a_f Q_{set} - (1 - a_f)S_n) + a_f(\omega^* - \omega_g), \tag{22}$$

where a_f is a parameter defining whether VSM is enabled ($a_f = 0$) when $V_g < 0.9$ p.u., or disabled ($a_f = 1$) when $V_g \geq 0.9$ p.u.

As discussed in the stability analysis of Section IV-B, the phase shift δ in the proposed controller (2) is bounded in the range $\delta \in [-\Delta\delta_m, \Delta\delta_m]$ independently from the function $g(Q_g, a_f, \omega_g)$ in (4). Hence, when the phase shift δ reaches the upper or lower limit of its value ($\Delta\delta_m$ or $-\Delta\delta_m$), from (13) and (14), it is clear that $P_g = 0$ in both cases while the reactive power becomes $Q_g = -S_n$ and $Q_g = S_n$, respectively, where S_n is the nominal apparent power of the inverter. This property, combined with the inherent current limitation, leads to the VSM of the proposed controller as explained below.

Table I
SYSTEM AND CONTROLLER PARAMETERS

Parameters	Values	Parameters	Values
L	7 mH	ω^*	2π x 50 rad/s
L_g	6 mH	l	1
r	0.5 Ω	r_g	0.5 Ω
C	11 μF	I_{max}	3 A
E^*	110 V	w_{min}	36.66 Ω
S_n	330 VA	Δw_m	531.66 Ω
c_w	380	K_e	10
c_δ	20	k_w, k_δ	1000
n	0.1667	m	0.0095

Considering a relatively stiff grid with $V_g = E^*$ and a small voltage drop between the capacitor voltage V_c and the grid voltage V_g, which can be neglected, then it yields

$$S = V_c I \approx V_g I \leq E^* I_{max} = S_n. \tag{23}$$

This expression actually provides the selection of the maximum current I_{max}, when the nominal apparent power of the inverter is known, i.e. $I_{max} = \frac{S_n}{E^*}$.

However, under grid faults, the grid voltage V_g drops by a percentage p and then according to (23), the proposed controller limits the apparent power below $(1-p)V_g I_{max}$. When VSM is enabled, i.e. $p > 0.1$, then $\alpha_f = 0$ and according to (4) and (22), the dynamics of the phase shift δ become

$$\dot{\delta} = c_\delta m (Q_g - S_n) \delta_q^{2l}. \tag{24}$$

Since the apparent power S of the inverter is limited below $(1-p)V_g I_{max}$ due to the current-limiting property, then in (24) there is

$$\dot{\delta} = c_\delta m (Q_g - S_n)\delta_q^{2l} \leq c_\delta m((1-p)V_g I_{max} - E^* I_{max})\delta_q^{2l} < 0.$$

This means that the phase shift δ will keep decreasing and since $\delta \in [-\Delta\delta_m, \Delta\delta_m]$, due to the bounded control structure of (4), there is $\delta \to -\Delta\delta_m$. This means that $Q_g \to Q_e = (1-p)E^* I_{max} < S_n$, i.e. the reactive power will be regulated to the maximum apparent power under the grid voltage drop. Obviously, the real power will automatically converge to zero since

$$P_g \to P_e = \sqrt{((1-p)E^* I_{max})^2 - Q_e^2} = 0.$$

This property indicates that opposed to existing algorithms that change both the real and reactive power references during faults, the proposed controller requires only a change in the phase shift dynamics of δ which are related to the reactive power while the real power will automatically drop to zero to allow maximum reactive power injection with an inherent current limitation and support the grid voltage. Furthermore, the change of the value of a_f during grid faults, changes only the function $g(Q_g, a_f, \omega_g)$ that is being integrated, while in conventional approaches the controller switches between dynamic controllers. Hence, the proposed controller keeps a unified structure with the same dynamic states at all times.

VI. EXPERIMENTAL VALIDATION

To verify the proposed control approach, a single-phase inverter with rated power $S_n = 330$ VA was experimentally tested using a modified version of the Texas Instrument (TI) Development Kit HV DC/AC Solar Inverter connected to a Chroma 61830 Regenerative Grid Simulator. The system and controller parameters are shown in Table I. A sinusoidal

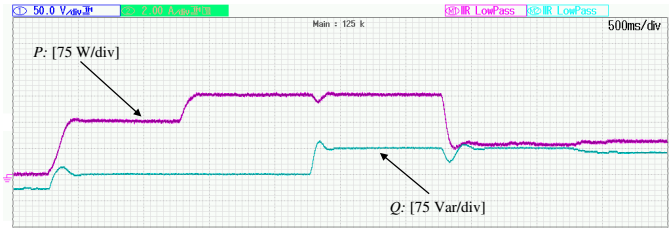

Figure 4. Operation under normal grid conditions

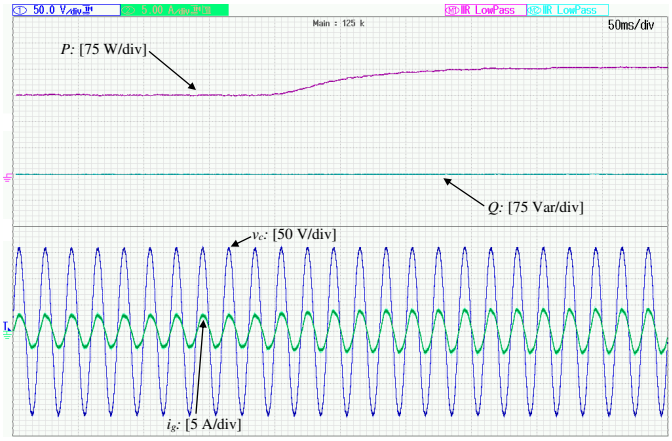

Figure 5. Transient response when P_{set} changes from 225 W to 350 W and $Q_{set} = 0$ (current-limiting property)

tracking algorithm PLL was used to obtain the required ω_g. The inverter switching frequency was 15 kHz while the proposed controller was implemented using a F28M35H52C1 DSP with a sampling frequency of 4 kHz. A lower sampling frequency (compared to the switching frequency) was selected, as commonly done when implementing the power control loops for inverter applications. For the droop functions, it is expected that at the nominal power S_n, a maximum of 5% deviation of the voltage and 1% deviation of the frequency is allowed [36]. Thus, since the $P \sim V$ and $Q \sim -\omega$ droop expressions are being used, the droop coefficients can be calculated as $n = \frac{0.05 K_e E^*}{S_n}$ for the real power droop and $m = \frac{0.01\omega^*}{S_n}$ for the reactive power droop, according to [5]. The real and reactive power is calculated using the measurements of the capacitor voltage v_c and the inverter current i, which are available at the TI inverter kit. For typical low-power inverter applications, the real and reactive power delivered to the grid (P_g and Q_g) are very close to the values of the real and reactive power delivered at the filter capacitor (P and Q), and hence P and Q can be used in the controller dynamics based on the measurements of v_c and i to simplify the implementation.

To verify both PQ-set control and PQ-droop control modes of the proposed controller, in Fig. 4 the following scenario is presented: At $t = 0.25$ s the inverter is connected to the grid and the real and reactive power reference values are set to 150 W and 0 Var, respectively. After 1 s, the real power reference is increased to 225 W and 1 s later the reactive power reference is increased to 75 Var. As it is shown in Fig. 4, both P and Q reach the desired values after a short transient. The real power droop control is enabled after 1 s and the real power drops in order to bring the output voltage of the inverter closer

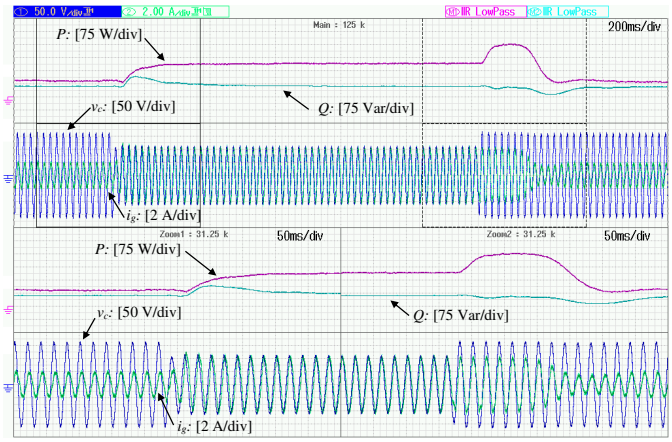

Figure 6. Operation under 37% drop of the grid voltage (110 V → 70 V)

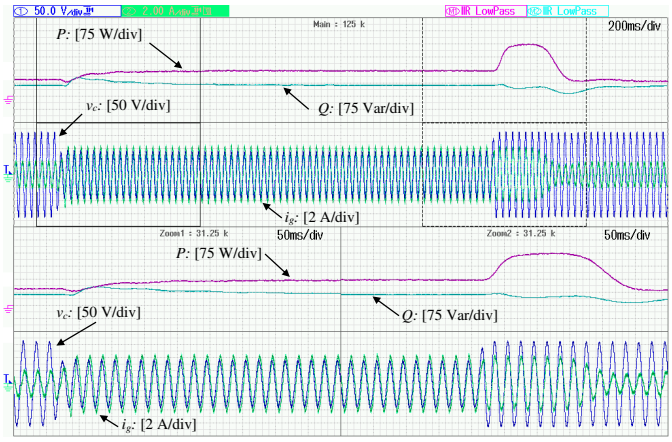

Figure 7. Operation under 50% drop of the grid voltage (110 V → 55 V)

to the rated value. Similarly, the reactive power droop control is enabled 1 s later and the injected reactive power drops since during that period the grid frequency was at 49.98 Hz, i.e. lower than the rated ω^*. In order to verify the current-limiting property ($I_{max} = 3$ A), in Fig. 5, the reference value of real power P_{set} is changed from 225 W to 350 W when the reactive power is zero. As it can be seen in Fig. 5, the RMS inverter current value is limited to almost 3 A and hence, the output real power is limited to slightly below 330 W, which corresponds to S_n for $Q = 0$. Thus, it is validated that the proposed controller protects the inverter from unrealistic power reference values. It is noteworthy that a THD around 5% is present at the grid current waveform. This is due to the fact that inner loop controllers are not considered in the controller implementation since the main goal of this brief is to propose the enhanced CLD controller and rigorously prove its theoretical current-limiting and stability properties for first time. However, when lower THD is required, conventional inner current and voltage control loops can be considered.

In order to test the proposed controller efficacy under grid faults, in Fig. 6, a drop of the grid voltage from the nominal value (110 V) to 70 V is applied at 340 ms. Due to the voltage drop, the real power increases and the current reaches its upper limit, leading the real power to its steady-state value $P_e = \sqrt{(1-\rho)^2 S_n^2 - Q_e^2} = \sqrt{0.63^2 330^2 - 62^2}\,\text{W} = 198\,\text{W}$. When the fault is cleared, both the real and reactive power return to their original values according to the droop control after a

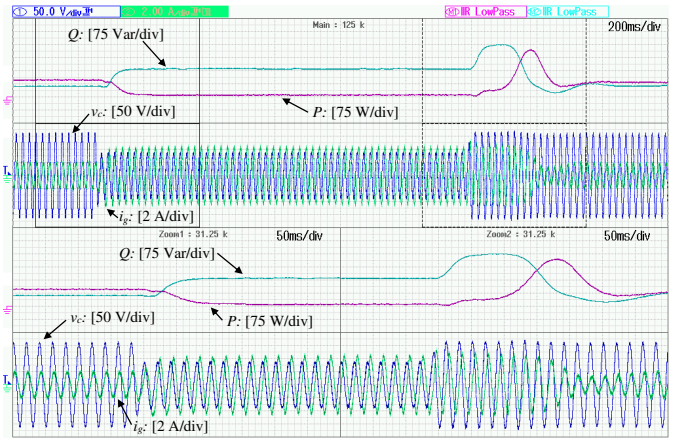

Figure 8. Operation under 50% drop of the grid voltage (110 V → 55 V) with voltage support enabled

short transient. One can see that during this short transient, the voltage returns to its nominal value instantly while the current remains at its maximum value for a short period of time. Hence, as it is depicted in Fig. 6, the apparent power is driven from the maximum available power during the fault to S_n, for a short time before returning to its original value, however it never exceeds S_n as required. At the bottom part of Fig. 6, the instances when the fault occurs and is being cleared are presented, where it can be clearly observed that the current remains below its maximum value during transients as well. A similar response is observed for a voltage drop of 50% of the nominal voltage in Fig. 7. Compared to the original CLD in [21], where the inverter current is limited to lower values under faults ($I_e \leq (1-\rho)\, I_{max}$), here, the proposed controller leads the inverter current to almost $I_{max} = 3$ A; thus utilizing the maximum power capacity of the inverter.

Since the maximum power utilization is now verified under grid faults, the voltage support mode can be enabled in the control system, as explained in Section V. Although the voltage support operation based on FRT requirements is mainly applied to three-phase inverters for MV and HV grids, very recently, the voltage support capability has shown increased interest for single-phase inverters connected to the LV grid as well [37]. The scenario of a 50% voltage drop is again tested while the inverter operates in the PQ-droop mode. As illustrated in Fig. 8, when the voltage sag occurs, the VSM algorithm is enabled and reactive power is maximized to support the voltage, while real power drops automatically to values close to 0 W, as described in Session V. As it can be observed in Fig. 8, when the fault is cleared, the real and reactive powers return to their original values. Note that the inverter current reaches the upper limit during the fault but never violates it, even during transients, as rigorously proven by the nonlinear ultimate boundedness theory in Section IV-A.

VII. Conclusions

A new current-limiting droop controller for grid-connected inverters was proposed in this brief to guarantee the maximum power utilization of the inverters under grid faults and closed-loop system stability. By addressing all limitations of the original CLD, the proposed enhanced version facilitates a rigorous asymptotic stability proof of any equilibrium point

within a given range. The proposed controller structure was further extended to provide voltage support under grid faults. Extensive experimental results verified the proposed control approach under normal and faulty grid conditions.

Although the inherent current limitation with voltage support capability and guaranteed closed-loop stability were the key contributions of this work, the validation at higher power levels and the optimal design of the LCL filter to further enhance the power quality are interesting topics for future research. These should be combined with an analysis of the effects of delays that may arise during the practical implementation of the proposed controller, both in the cases of single and cascaded control design (including inner current and voltage control loops).

REFERENCES

[1] Y. Xue and J. M. Guerrero, "Smart inverters for utility and industry applications," in *Proceedings of PCIM Europe 2015; International Exhibition and Conference for Power Electronics, Intelligent Motion, Renewable Energy and Energy Management*, May 2015, pp. 1–8.

[2] National Grid Electricity Transmission plc. (2016) The grid code.

[3] J. M. Guerrero, J. C. Vasquez, J. Matas, L. G. de Vicuna, and M. Castilla, "Hierarchical control of droop-controlled ac and dc microgrids-a general approach toward standardization," *IEEE Transactions on Industrial Electronics*, vol. 58, no. 1, pp. 158–172, Jan 2011.

[4] H. Liu, P. C. Loh, X. Wang, Y. Yang, W. Wang, and D. Xu, "Droop control with improved disturbance adaption for a pv system with two power conversion stages," *IEEE Transactions on Industrial Electronics*, vol. 63, no. 10, pp. 6073–6085, Oct 2016.

[5] Q. C. Zhong and Y. Zeng, "Universal droop control of inverters with different types of output impedance," *IEEE Access*, vol. 4, pp. 702–712, 2016.

[6] C. C. Chang, D. Gorinevsky, and S. Lall, "Stability analysis of distributed power generation with droop inverters," *IEEE Transactions on Power Systems*, vol. 30, no. 6, pp. 3295–3303, Nov 2015.

[7] B. P. Loop, S. D. Sudhoff, S. H. Zak, and E. L. Zivi, "Estimating regions of asymptotic stability of power electronics systems using genetic algorithms," *IEEE Transactions on Control Systems Technology*, vol. 18, no. 5, pp. 1011–1022, Sept 2010.

[8] L. Huang, H. Xin, Z. Wang, K. Wu, H. Wang, J. Hu, and C. Lu, "A virtual synchronous control for voltage-source converters utilizing dynamics of dc-link capacitor to realize self-synchronization," *IEEE Journal of Emerging and Selected Topics in Power Electronics*, vol. 5, no. 4, pp. 1565–1577, Dec 2017.

[9] J. Schiffer, R. Ortega, A. Astolfi, J. Raisch, and T. Sezi, "Conditions for stability of droop-controlled inverter-based microgrids," *Automatica*, vol. 50, no. 10, pp. 2457 – 2469, 2014.

[10] J. W. Simpson-Porco, F. Dorfler, and F. Bullo, "Voltage stabilization in microgrids via quadratic droop control," *IEEE Transactions on Automatic Control*, vol. 62, no. 3, pp. 1239–1253, March 2017.

[11] J. W. Simpson-Porco, F. Dörfler, and F. Bullo, "Synchronization and power sharing for droop-controlled inverters in islanded microgrids," *Automatica*, vol. 49, no. 9, pp. 2603–2611, 2013.

[12] J. Schiffer, T. Seel, J. Raisch, and T. Sezi, "Voltage stability and reactive power sharing in inverter-based microgrids with consensus-based distributed voltage control," *IEEE Transactions on Control Systems Technology*, vol. 24, no. 1, pp. 96–109, Jan 2016.

[13] A. Camacho, M. Castilla, J. Miret, A. Borrell, and L. G. de Vicuna, "Active and reactive power strategies with peak current limitation for distributed generation inverters during unbalanced grid faults," *IEEE Transactions on Industrial Electronics*, vol. 62, no. 3, pp. 1515–1525, March 2015.

[14] X. Guo, W. Liu, and Z. Lu, "Flexible power regulation and current-limited control of the grid-connected inverter under unbalanced grid voltage faults," *IEEE Transactions on Industrial Electronics*, vol. 64, no. 9, pp. 7425–7432, Sept 2017.

[15] I. Sadeghkhani, M. E. H. Golshan, J. M. Guerrero, and A. Mehrizi-Sani, "A current limiting strategy to improve fault ride-through of inverter interfaced autonomous microgrids," *IEEE Transactions on Smart Grid*, vol. 8, no. 5, pp. 2138–2148, Sept 2017.

[16] X. Lu, J. Wang, J. M. Guerrero, and D. Zhao, "Virtual-impedance-based fault current limiters for inverter dominated ac microgrids," *IEEE Transactions on Smart Grid*, vol. 9, no. 3, pp. 1599–1612, May 2018.

[17] A. D. Paquette and D. M. Divan, "Virtual impedance current limiting for inverters in microgrids with synchronous generators," *IEEE Transactions on Industry Applications*, vol. 51, no. 2, pp. 1630–1638, March 2015.

[18] A. Tilli and C. Conficoni, "Control of shunt active filters with actuation and current limits," *IEEE Transactions on Control Systems Technology*, vol. 24, no. 2, pp. 644–653, March 2016.

[19] G. C. Konstantopoulos and Q. Zhong, "Current-limiting dc/dc power converters," *IEEE Transactions on Control Systems Technology*, vol. 27, no. 2, pp. 855–863, March 2019.

[20] N. Bottrell and T. C. Green, "Comparison of current-limiting strategies during fault ride-through of inverters to prevent latch-up and wind-up," *IEEE Trans. Power Electron.*, vol. 29, no. 7, pp. 3786–3797, 2014.

[21] Q. C. Zhong and G. C. Konstantopoulos, "Current-limiting droop control of grid-connected inverters," *IEEE Transactions on Industrial Electronics*, vol. 64, no. 7, pp. 5963–5973, July 2017.

[22] ENTSO-E. (2013) Nework code for requirements for grid connection - applicable to all generators.

[23] M. A. Garnica López, J. L. García de Vicuña, J. Miret, M. Castilla, and R. Guzmán, "Control strategy for grid-connected three-phase inverters during voltage sags to meet grid codes and to maximize power delivery capability," *IEEE Transactions on Power Electronics*, vol. 33, no. 11, pp. 9360–9374, Nov 2018.

[24] A. G. Paspatis, G. C. Konstantopoulos, M. Mayfield, and V. C. Nikolaidis, "Current-limiting droop controller with fault-ride-through capability for grid-tied inverters," in *2017 IEEE PES Innovative Smart Grid Technologies Conference Europe (ISGT-Europe)*, Sept 2017, pp. 1–6.

[25] T. Orlowska-Kowalska, F. Blaabjerg, and J. Rodriguez, *Advanced and Intelligent Control in Power Electronics and Drives*. New York, NY, USA: Springer-Verlag, 2014.

[26] Bundesverband der Energie und Wasserwirtschaft (BDEW). (2008) Technical guideline: Generating plants connected to the medium-voltage network.

[27] X. Zhao, J. M. Guerrero, M. Savaghebi, J. C. Vasquez, X. Wu, and K. Sun, "Low-voltage ride-through operation of power converters in grid-interactive microgrids by using negative-sequence droop control," *IEEE Transactions on Power Electronics*, vol. 32, no. 4, pp. 3128–3142, April 2017.

[28] P. Piya, M. Ebrahimi, M. Karimi-Ghartemani, and S. A. Khajehoddin, "Fault ride-through capability of voltage-controlled inverters," *IEEE Transactions on Industrial Electronics*, vol. 65, no. 10, pp. 7933–7943, Oct 2018.

[29] G. C. Konstantopoulos, Q. C. Zhong, B. Ren, and M. Krstic, "Bounded integral control of input-to-state practically stable nonlinear systems to guarantee closed-loop stability," *IEEE Transactions on Automatic Control*, vol. 61, no. 12, pp. 4196–4202, Dec 2016.

[30] J. M. Guerrero, J. Matas, L. G. de Vicuna, M. Castilla, and J. Miret, "Decentralized control for parallel operation of distributed generation inverters using resistive output impedance," *IEEE Transactions on Industrial Electronics*, vol. 54, no. 2, pp. 994–1004, April 2007.

[31] G. C. Konstantopoulos, Q.-C. Zhong, and W.-L. Ming, "PLL-less nonlinear current-limiting controller for single-phase grid-tied inverters: Design, stability analysis and operation under grid faults," *IEEE Trans. Ind. Electron.*, vol. 63, no. 9, pp. 5582–5591, Sept 2016.

[32] H. K. Khalil, *Nonlinear Systems*. Prentice Hall, 1996.

[33] J. Schiffer, D. Zonetti, R. Ortega, A. M. Stanković, T. Sezi, and J. Raisch, "A survey on modeling of microgrids—from fundamental physics to phasors and voltage sources," *Automatica*, vol. 74, pp. 135 – 150, 2016.

[34] Q.-C. Zhong and D. Boroyevich, "A droop controller is intrinsically a phase-locked loop," in *Proc. of the 39th Annual Conference of the IEEE Industrial Electronics Society, IECON 2013*, Vienna, Austria, Nov. 2013, pp. 5916–5921.

[35] J. D. Glover, M. S. Sarma, and T. J. Overbye, *Power System Analysis and Design*. Cengage Learning, 2012.

[36] "Wind integration: International experience, wp2: Review of grid codes," Australian Energy Market Operator, Tech. Rep., 2011.

[37] Y. Yang, F. Blaabjerg, and H. Wang, "Low-voltage ride-through of single-phase transformerless photovoltaic inverters," *IEEE Transactions on Industry Applications*, vol. 50, no. 3, pp. 1942–1952, May 2014.